NANO LETTERS

Letter

pubs.acs.org/NanoLett

Doubling the Efficiency of Third Harmonic Generation by Positioning ITO Nanocrystals into the Hot-Spot of Plasmonic Gap-Antennas

Bernd Metzger,[†] Mario Hentschel,*[,†,‡] Thorsten Schumacher,[†,‡,§] Markus Lippitz,[†,‡,§] Xingchen Ye,[∥] Christopher B. Murray,[∥,#] Bastian Knabe,[⊥,○] Karsten Buse,[⊥,○] and Harald Giessen[†]

[†]4th Physics Institute and Research Center SCoPE, University of Stuttgart, Pfaffenwaldring 57, 70569 Stuttgart, Germany

[‡]Max Planck Institute for Solid State Research, Heisenbergstr. 1, 70569 Stuttgart, Germany

[§]Experimental Physics III, University of Bayreuth, Universitätsstr. 30, 95447 Bayreuth, Germany

[∥]Department of Chemistry and [#]Department of Materials Science and Engineering, University of Pennsylvania, 231 South 34th Street, Philadelphia, Pennsylvania 19104-6323, United States

[⊥]Department of Microsystems Engineering, University of Freiburg, Georges-Köhler-Allee 102, 79110 Freiburg, Germany

[○]Fraunhofer Institute for Physical Measurement Techniques IPM, Heidenhofstr. 8, 79110 Freiburg, Germany

Supporting Information

ABSTRACT: We incorporate dielectric indium tin oxide nanocrystals into the hot-spot of gold nanogap-antennas and perform third harmonic spectroscopy on these hybrid nanostructure arrays. The combined system shows a 2-fold increase of the radiated third harmonic intensity when compared to bare gold antennas. In order to identify the origin of the enhanced nonlinear response we perform finite element simulations of the nanostructures, which are in excellent agreement with our measurements. We find that the third harmonic signal enhancement is mainly related to changes in the linear optical properties of the plasmonic antenna resonances when the ITO nanocrystals are incorporated. Furthermore, the dominant source of the third harmonic is found to be located in the gold volume of the plasmonic antennas.

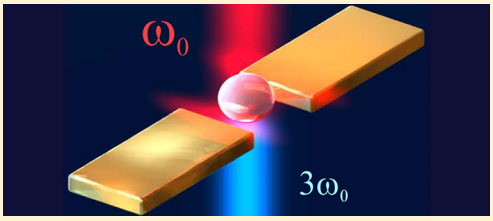

KEYWORDS: *Nano-optics, plasmonics, nonlinear optics, spectroscopy, third harmonic generation*

The optical properties of nanoscale matter differ strongly from those of their bulk counterparts. The reasons can be manifold: While the mere reduction in size leads to a massively reduced light-matter interaction volume, resonant and confinement effects, such as Mie resonances[1] or surface plasmon polariton modes, can as well significantly alter the optical properties. Let us consider as an example the nonlinear optical response of bulk crystals: When illuminated with an intense light field they can exhibit extremely high conversion efficiencies for second harmonic (SH) and third harmonic (TH) generation, respectively.[2] For a number of applications, such as optical biolabels,[3−6] as well as from a fundamental physics standpoint, it is very intriguing to study these effects in nanocrystals.[7] However, any attempt to study their nonlinear optical response will be largely hampered by the extremely small sample volume, that is, the small conversion volume, and potentially by the limited electric field strength of the external light field.[8]

Both challenges appear to be uniquely addressed by plasmonics,[9−12] another field of nanoscale light matter interaction. Plasmonic nanoantennas exhibit extremely large resonant light interaction cross sections, much larger than their geometrical size.[10] Moreover, because of their subwavelength dimension they confine far-field radiation into subwavelength volumes, leading to significantly enhanced electric near-fields. It has been shown that purely plasmonic systems exhibit significant conversion efficiencies for SH generation[13−15] and TH generation,[16,17] as well as other nonlinear optical processes,[18,19] in particular when taking the small structure volume into account.[20−22] Consequently, researchers have envisioned the combination of well-known and highly efficient bulk nonlinear dielectrics with plasmonic nanoantennas for further enhancement and even more efficient nonlinear light sources at the nanoscale.[23−30]

In this letter we realize and investigate exactly such a system. First, we demonstrate the fabrication of hybrid indium tin oxide (ITO) nanocrystal-incorporated plasmonic gap-antennas using a two-step electron beam lithography process. The ITO nanocrystals possess a high nonlinear optical susceptibility $\chi^{(3)}$.[30,31] Second, we investigate the hybrid nanostructure arrays by means of third harmonic spectroscopy and observe in experiment and in simulation doubling of the third harmonic response of the hybrid system, when comparing to the TH response of an identical bare plasmonic gap-antenna array, without ITO nanocrystals. Third, we identify the origin of the third harmonic signal enhancement, which is mainly related to

Received: March 11, 2014
Revised: April 9, 2014
Published: April 14, 2014

ACS Publications © 2014 American Chemical Society

changes in the linear optical properties and the lifetime of the plasmonic antenna resonances.

In our experiments and simulations we utilize arrays of dimer nanoantennas consisting of two identical gold rods separated by a small gap, cf. Figure 1. Illuminating the nanostructure arrays

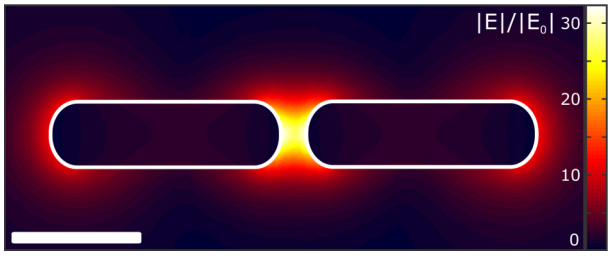

Figure 1. Simulation of the electric near-field enhancement $|\mathbf{E}|/|\mathbf{E}_0|$ inside and in the surroundings of a plasmonic gap-antenna. The field distribution is shown for the plane symmetrically cutting the antenna and for resonant excitation. The scale bar corresponds to 100 nm.

with electromagnetic plane waves polarized along the long-axis of the gap-antennas excites the hybridized symmetric plasmonic mode, located in the near-infrared spectral region at about 1000 nm. To estimate the electric field enhancement $|\mathbf{E}|/|\mathbf{E}_0|$ associated with this plasmonic mode, we perform finite element simulations of the structures, where $\mathbf{E}$ and $\mathbf{E}_0$ are defined as the local electric field amplitude and the incoming electric far-field amplitude, respectively. For the simulations we utilize a commercial software package (Comsol Multiphysics). Therein, the structures are defined on a substrate with a constant refractive index of $n = 1.5$, and for the optical properties of gold we use the data of Johnson and Christy.[32] Figure 1 shows the electric field enhancement $|\mathbf{E}|/|\mathbf{E}_0|$ for resonant plane wave excitation of our plasmonic gap-antenna. As expected, the strongest electric field enhancement of about 20 to 30 is observed in the gap region of the dimer nanoantenna, which is commonly referred to as the antenna hot-spot. This hot-spot is generally expected to be the major source of any nonlinear signal and is in particular the ideal position for a selective incorporation of a nonlinear dielectric.[33,34]

In order to experimentally study the proposed system we developed a process for the selective filling of the antenna gaps with different kinds of nanoparticles. The fabrication of the hybrid nanostructure arrays works via a two-step electron beam exposure[35] and a subsequent so-called squeegee process.[36,37] In a first step the nanoantennas as well as alignment marks are defined in a double layer poly(methyl methacrylate) (PMMA) resist on a fused silica substrate (Suprasil, Heraeus), followed by the evaporation of a 2 nm Cr adhesion layer and a 40 nm gold layer and the subsequent lift-off of the resist. Afterward, the sample is once again coated with a double layer of PMMA resist, and the alignment marks are used to selectively open resist apertures on top of the nanoantenna gaps. Subsequently, nanoparticles can be transferred into the apertures from a nanoparticle solution. In our case, monodisperse ITO nanocrystals have been synthesized according to literature methods,[38] resulting in a mean crystal diameter of 6 nm, suspended in hexane. A droplet of the concentrated nanocrystal-hexane solution is deposited onto the resist and swept across the sample surface by a cut piece of polydimethylsiloxane (PDMS). The particles are dragged along with the meniscus of the slowly evaporating hexane solution and deposited into the resist openings.[37] Once the hexane is nearly fully evaporated, the remaining nanocrystals are dragged to the rim of the substrate and away from the gold nanostructures in order to prevent clustering in the structured areas. Subsequently, the sample is placed top-down on additional glass slides in an acetone beaker to remove the PMMA resist mask and the excess nanocrystals. The final nanoantenna arrays have a size of $90 \times 90\ \mu m^2$, with an excellent filling ratio of the antenna feed gaps; see scanning electron micrographs in Figure 2. The

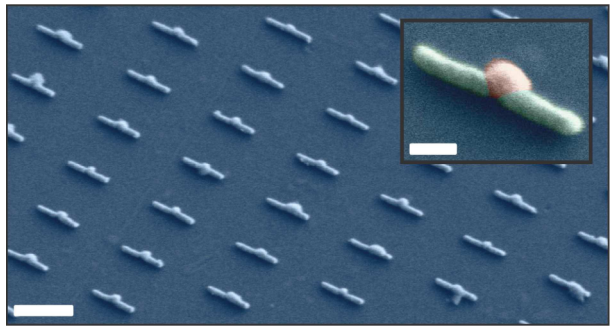

Figure 2. Colored scanning electron micrograph (SEM) of a hybrid ITO nanocrystal-incorporated plasmonic gap-antenna array. The inset shows an SEM of a single antenna element. The individual gap-antenna elements consist of two identical gold rods, with a height, a width, and a length of about 40, 50, and 180 nm, respectively. The gap distance is about 20 nm. The scale bar is 500 nm in the overview and 100 nm in the inset, respectively.

following measurements of the plasmonic nanoantenna arrays are intrinsically ensemble measurements and might therefore be influenced by inhomogeneous effects, in particular by size and shape variations within an antenna array. However, we find good agreement between measured and simulated far-field spectra, which underlines the excellent homogenity of the fabricated nanostructure arrays.

First of all the incorporation of the high refractive index ITO nanocrystals into the hot-spot of the gold gap-antennas influences the plasmonic mode of the nanoantennas since these are highly sensitive to changes in the dielectric environment. In particular, the resonance frequency ω_0 of the plasmonic mode shifts to lower frequencies due to the increase in the outer effective dielectric constant. Therefore, it is necessary to perform spectrally resolved nonlinear spectroscopy to ensure the resonant excitation of the antenna arrays and to determine the spectral position of highest conversion efficiency.[39] Hence, we focus sub-30 fs laser pulses polarized along the long antenna axis and tunable between 900 and 1200 nm with a 75 mm focal length achromatic lens on the nanostructure arrays. Subsequently, the generated TH signals radiated in forward direction, which are as well polarized along the antenna axis, are recollimated, focused into a grating spectrometer, and measured with an attached Peltier-cooled CCD camera. Finally, the measured TH spectra are spectrally integrated, yielding a scalar value describing the TH intensity. All TH measurements are normalized to a TH signal, which is generated at the interface of the bare substrate. Thereby, we eliminate the influence of any wavelength-dependent components, changing beam parameters, or the detector efficiency.[40]

Figure 3a depicts the spectroscopic results for one exemplary bare (green) and hybrid (orange) antenna array. The solid lines correspond to the measured linear extinction spectra of the antenna arrays, whereas the data points (diamonds) represent the normalized TH intensities. The linear extinction spectrum

dx.doi.org/10.1021/nl500913t | Nano Lett. 2014, 14, 2867−2872

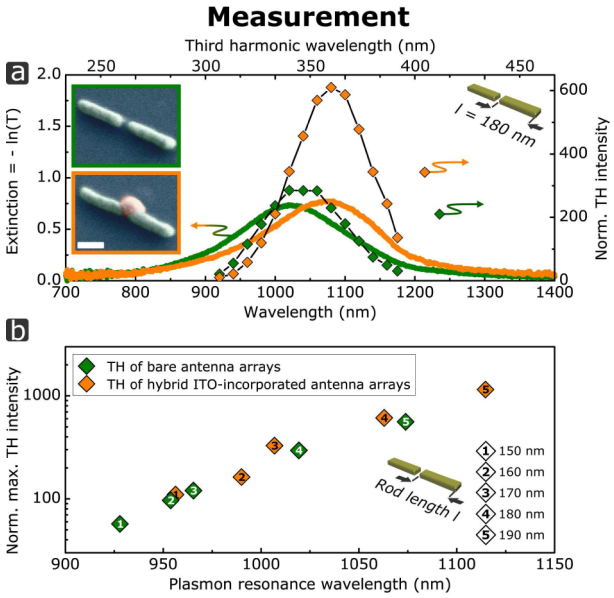

Figure 3. (a) Third harmonic spectroscopy of bare (green) and hybrid ITO nanocrystal-incorporated (orange) plasmonic gap-antenna arrays, with an antenna rod length l of about 180 nm. The solid lines correspond to the measured extinction spectra, while the data points are the measured TH intensities plotted over the fundamental excitation wavelength. The top axis shows the corresponding TH wavelength. (b) Maximum of the measured TH intensities of different bare (green) and ITO nanocrystal-incorporated (orange) gap-antenna arrays with different rod length l plotted over their corresponding plasmon resonance wavelength. Data points with identical labeling correspond to an equal antenna length l, which is given in the right corner of the graph.

of the bare gap-antenna array (green) is characterized by a single Lorentzian peak associated with its plasmon resonance at around 1025 nm. As reported in earlier work,[41−43] we find the peak of the TH conversion efficiency (green diamonds) close yet slightly red-shifted with respect to the peak of its far-field extinction spectrum. As mentioned above the incorporation of the ITO nanocrystals leads to a significant red-shift of the extinction peak by about 45 nm. The origin of the red-shift is the increase of the dielectric constant ϵ_m of the environment, which changes in the gap region, that is, the ITO volume from $\epsilon_{m,AIR} = 1$ of air to about $\epsilon_{m,ITO} \approx 2.9$ of the ITO.[44] Consequently, the peak of the TH conversion efficiency (orange diamonds) shifts together with the linear spectrum to longer wavelengths by about the same value. The maximum TH conversion efficiency is about a factor of 2 larger when compared to that of the bare gap-antenna arrays.

In order to further investigate the role of the ITO nanocrystals in the measured enhancement of the TH conversion efficiency, we tune the spectral characteristics of the gap-antennas by varying the length l of the two gold rods from about 150 to about 190 nm, in a step size of 10 nm. As before, we measured the TH spectra of the bare as well as the hybrid ITO nanocrystal-incorporated antenna arrays. The measured linear and TH signal spectra exhibit very similar behavior as the exemplary one shown in Figure 3a. For clarity, in Figure 3b, we only plot the maximum TH signal strength for each antenna array versus the spectral position of its plasmonic resonance (green, bare; orange, nanocrystal-incorporated). We observe a monotonic increase of the TH intensity radiated from all measured antenna arrays when plotted over their corresponding plasmon resonance wavelength. In particular, we find that the TH signal increases by about an order of magnitude in the considered wavelength range. Remarkably, the TH maxima of the hybrid nanocrystal-incorporated gap-antenna arrays and the bare antenna arrays follow the same trend, not only qualitatively but also quantitatively. The measured data suggests that only the spectral position of the plasmonic resonance determines the maximum TH signal. In contrast, if there was a significant contribution of the ITO nanocrystals to the overall TH signal, the bare and the ITO nanocrystal-incorporated antenna arrays should form two distinct subsets in Figure 3b, with the latter having a higher overall TH signal. The observation that they form a single indistinguishable set is a strong indication that a contribution of the ITO nanocrystals to the overall TH intensity is not the main reason for the observed increased TH conversion efficiency. However, it is known that the linear optical properties of a plasmonic system have crucial influence on its nonlinear optical response. In particular, the spectral position of the plasmon resonance frequency ω_0 and the damping γ, that is, the quality factor Q or the lifetime τ of the resonator, are of crucial importance.[39,43,45]

In order to determine the origin of the TH signal enhancement between hybrid ITO nanocrystal-incorporated and bare gap-antenna arrays we perform finite element simulations (Comsol Multiphysics) of the nanostructures, which were already used for the calculation of the absolute electric field enhancement in the gap-antennas in Figure 1. The TH signal radiated from the hybrid plasmonic gap antennas is directly related to the TH polarization $\mathbf{P}^{(3)}_{TH} = \epsilon_0\chi^{(3)}(\omega)\mathbf{E}^3$ in the gold and the ITO volume, respectively. However, quantitative and wavelength-dependent literature values for the third order susceptibilities $\chi^{(3)}(\omega)$ for gold and ITO are hardly available. Hence, instead we consider the linear polarization $\mathbf{P}(\mathbf{r},\omega)$ in the gold and the ITO volume since the third power of the linear polarization is proportional to the TH polarization $\mathbf{P}^{(3)}_{TH} \propto \mathbf{P}(\mathbf{r},\omega)^3$ and since this gives a good estimate for the different contributions to the TH response.[2,46]

In Figure 4a we show the x-component of the cubed linear polarization $\mathbf{P}(\mathbf{r},\omega)^3$ within a bare and a hybrid ITO nanocrystal-incorporated gold gap-antenna (each at the spectral peak position of their respective plasmonic resonances) since only the x-components (along the antenna axis) of the TH near-field polarizations contribute to the TH far-field amplitude polarized along the gap-antennas. Two important observations can be made: (1) In case of the bare gap-antenna the strongest TH polarization is observed in the region of highest plasmonic current density, namely, close to the surface in the center region of the gold rods. In particular, no TH polarization is observed in the gap region, as there is no material present that could carry any nonlinear polarization. (2) In the case of the ITO nanocrystal-incorporated gap-antenna we observe a distinct enhancement of the TH near-field polarization inside the gold volume. However, compared to the TH polarization in the gold we observe only a very weak TH polarization inside of the ITO volume. Of course, the TH near-field polarization in the ITO volume becomes significantly enhanced by the presence of the plasmonic antenna; however, *compared to the TH polarization in the gold volume this is only a minor contribution the overall TH response*. The strong difference of the TH polarizations in both materials is directly linked to their linear optical properties, namely, to the weak linear polar-

dx.doi.org/10.1021/nl500913t | *Nano Lett.* 2014, 14, 2867−2872

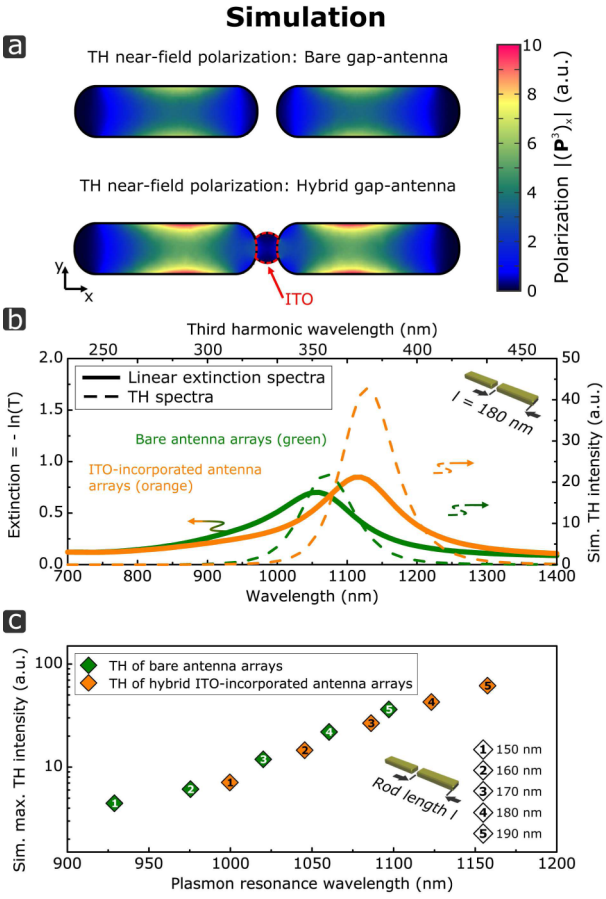

Figure 4. (a) Simulations of the *x*-component of the TH near-field polarization in a bare and a hybrid ITO nanocrystal-incorporated gold gap-antenna. The red-rimmed area indicates the ITO volume. (b) Simulated linear extinction spectra (solid lines) and simulated TH intensities (dashed) for bare (green) and ITO nanocrystal-incorporated (orange) gap-antennas plotted over the fundamental wavelength. The top axis shows the corresponding TH wavelength. (c) Maximum of the simulated TH intensities of different bare (green) and ITO-incorporated (orange) gap-antenna arrays with different gap-antenna length *l*.

izability of a dielectric material like ITO as compared to a metal such as gold.

This observation confirms what we already suspected: The overall TH response seems to be dominated by the TH polarization in the gold rather than by the optical nonlinearity of the ITO. However, since the simulated polarization maps cannot directly be measured we need to transfer this information into experimentally accessible quantities, which are the linear extinction spectra as well as the TH signal strength. Therefore, we calculate the TH signals radiated from the bare and the hybrid gap-antenna arrays by integrating the TH near-field polarizations over the volume V of the gold antennas. In particular, we neglect all TH polarizations in the ITO volume since they will contribute only a minute TH signal to the overall TH intensity, due to the small TH polarization and also due to the small volume of the ITO as compared to the gold. Hence, the TH electric field amplitude $\mathbf{E}_{\mathrm{TH}}(\omega)$ radiated into the far-field is given by[46]

$$\mathbf{E}_{\mathrm{TH}}(\omega) \propto \omega_{\mathrm{TH}} \int_V \mathbf{P}(\mathbf{r}, \omega)^3 \mathrm{d}r^3 \tag{1}$$

where

$$\mathbf{P}(\mathbf{r}, \omega)^3 = (P_x^2 + P_y^2 + P_z^2)\cdot\mathbf{P}(\mathbf{r}, \omega) \tag{2}$$

ω_{TH} is the TH frequency, and P_x, P_y, and P_z are the complex valued Cartesian components of the linear polarization $\mathbf{P}(\mathbf{r},\omega)$. Figure 4b depicts the simulated linear (solid) and TH spectra (dashed) for a bare (green) and a hybrid (orange) gap-antenna array with a rod length l of 180 nm calculated via eq 1. For the TH spectra, similar to Figure 4a we only evaluated the *x*-component of the TH electric field amplitude in eq 1 since this component corresponds to the measured TH polarization along the gap-antennas. Despite the fact that we have completely neglected the TH response of ITO (only taking into account its purely linear dielectric contribution), we find excellent agreement between the simulation results shown in Figure 4b and the corresponding experimental spectra in Figure 3a. In particular, the linear resonance positions are reproduced, as is the red-shift between the maximum TH signal and the linear plasmon peak. Even more importantly, the enhancement by a factor of about two of the maximum TH signal by incorporation of the ITO nanocrystals is as well observed.

The simulations are also capable to capture the trend shown in Figure 3b: We simulated the linear spectra and the TH spectra for different rod lengths l, ranging from 150 to 190 nm and plotted in Figure 4c the maximum TH intensity of each antenna array depending on their corresponding plasmon resonance wavelength. As in the experiment we observe a monotonic increase of the maximum TH intensity by about an order of magnitude over the whole considered wavelength range. In summary, the fact that all characteristic features of the experimental results are well reproduced while disregarding any optical nonlinearity of the ITO nanocrystals is clear proof of a at-best minute contribution of the ITO nanocrystals to the overall TH response.

One might ask why we observe an increase in the TH signal strength at all. More importantly, can one intuitively understand the physical processes involved? The origin of the TH enhancement has to be correlated to an increased near-field enhancement or equivalently to an increased dipole moment $\mathbf{p}$ of the plasmonic oscillations in the gold gap-antennas. When the ITO nanocrystals are incorporated in the antenna gaps or the rods of the gap-antennas are elongated, the dielectric constant ϵ_m of the environment or the volume V of the gap-antennas is increased, respectively. Both partly enhance the dipole moment $\mathbf{p}$ of the plasmonic resonance.[9] In a full electrodynamic solution several parameters, which influence the overall dipole moment $\mathbf{p}$ in plasmonic antennas, vary simultaneously and cannot be completely disentangled.

However, we want to stress two important quantities of the plasmon resonance for the TH response, which are the plasmon resonance frequency ω_0 and the damping constant γ. It can be shown in terms of a harmonic oscillator model, which has proven to describe the nonlinear response of bare plasmonic nanoantennas well,[39,43] that the absolute value of the dipole moment $|\mathbf{p}|$ of the plasmon resonance at its peak position is in good approximation ($\gamma \ll \omega_0$) inversely proportional to these quantities: $|\mathbf{p}| \propto 1/(\omega_0\gamma)$. Since the TH intensity scales with the sixth power of the plasmonic dipole moment $\mathbf{p}$, the TH signal should critically depend on these quantities and increase with decreasing ω_0 and γ.[2,43]

If this reasoning is correct, we expect a monotonic decrease of the linewidth $\Delta\omega_{\mathrm{FWHM}}$, which is proportional to the damping constant γ, for red-shifted antenna arrays, irrespective of whether the shift is induced due to the presence of the

dx.doi.org/10.1021/nl500913t | Nano Lett. 2014, 14, 2867−2872

nanocrystals or due to an elongation of the gap-antenna length *l*. Hence, we extracted the linewidth $\Delta\omega_{FWHM}$ of the plasmonic resonances by fitting the measured and the simulated linear extinction spectra with a Lorentzian function and display them in dependence of the corresponding plasmon resonance wavelength in Figure 5. In measurement and in simulation

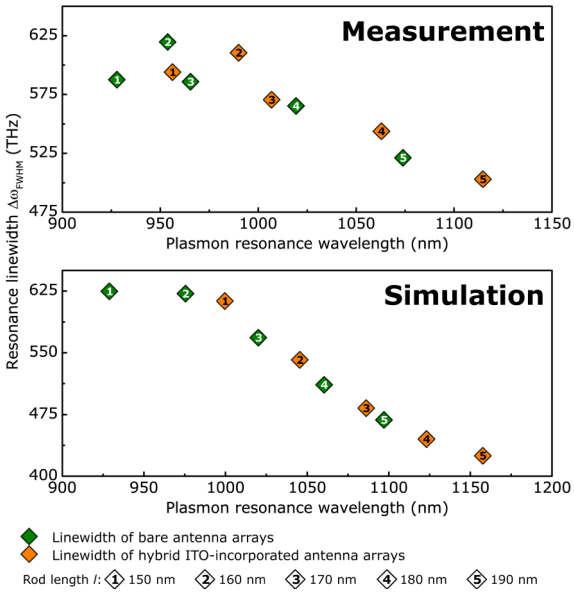

Figure 5. Linewidth $\Delta\omega_{FWHM}$ of plasmon resonances of measured (top) and simulated (bottom) linear spectra plotted over the plasmon resonance wavelength for bare (green) and ITO nanocrystal-incorporated (orange) gap-antenna arrays with different gap-antenna length *l*.

we observe a monotonic decrease of the resonance linewidth $\Delta\omega_{FWHM}$ with the plasmon resonance wavelength. Noteworthy, the linewidth $\Delta\omega_{FWHM}$ of the bare (green) and the hybrid (orange) gap-antenna arrays follow quantitatively the same behavior, and the two sets are indistinguishable.

Most likely, the origin of the reduced resonance linewidth $\Delta\omega_{FWHM}$ can be attributed to an increased spectral distance with respect to d-band interband absorption, which occurs for gold in the visible regime. At the same time an increase of radiative losses, which could be expected for the increased volume of the elongated rods of the gap-antenna, seems to not play a major role for our structures.[47]

Thus, for the bare and the hybrid nanostructure arrays the increase in the TH signal strength is mainly related to a decrease of the resonance frequency ω_0 and a decrease in the linewidth $\Delta\omega_{FWHM}$ or the damping constant γ, which lead to an enhanced dipole moment $\mathbf{p}$ of the red-shifted plasmon resonances and therefore to increased generation of TH light.

To summarize, we developed a new method for selectively filling nanoparticles from solution into the hot-spot of plasmonic gap-antennas and studied the TH response of corresponding hybrid ITO nanocrystal-incorporated plasmonic gap-antenna arrays. We observed an enhancement of the TH signals radiated from the hybrid gap-antenna arrays by about a factor of 2 when comparing them to the TH signals of identical bare plasmonic gap-antenna arrays. A close study revealed that the enhanced TH signal strength is mainly related to changes in the linear optical properties of the respective antenna arrays. The incorporation of the ITO nanocrystals leads a red-shift of the plasmon resonance and therefore to a decrease of the resonance frequency ω_0 and the linewidth $\Delta\omega_{FWHM}$. Both decreasing quantities increase the dipole moment $\mathbf{p}$ of the plasmon resonances and lead ultimately to the observed increase in the TH signal strength. Hence, the TH response of our plasmonic gap-antennas can be boosted by either increasing the gap-antenna length or by the deposition of dielectric material around the gold nanostructures, which red-shifts the plasmon resonance and therefore increases the TH signal strength. Furthermore, our TH signal is found to be nearly exclusively generated in the gold volume and not inside the ITO nanocrystals,[48] which is directly related to the higher *linear* polarizability and the third-order susceptibilitiy of gold when compared to that of ITO.

Despite the fact that we were not able to resolve an enhanced TH signal from the dielectric material itself, the overall concept is still promising. We believe that other nonlinear materials with an even higher linear polarizability and also higher third-order susceptibility should give a distinct contribution to the overall TH response when incorporated into the hot-spot of plasmonic nanoantennas, which then also should allow for enhancing the TH response at a certain wavelength. An increase of the plasmon lifetime, e.g., by using more complex structures[46,49,50] or by the implementation of single crystalline metals[51] should even further boost the nonlinear optical response. Furthermore, in this work we utilized a third order nonlinear effect, which can be observed in isotropic materials as it is not subject to symmetry restrictions, such as even order processes.[52] It has indeed been demonstrated that the use of SH generation in mixed systems composed of split ring resonators and crystalline gallium arsenide substrates allows for the disentanglement of contributions stemming from the gold structures itself as well as from the crystalline substrate.[26,53] Similarly, one could incorporate noninversion symmetric materials, such as lithium niobate, in the hot-spot of the nanoantennas and study the radiated SH rather than TH signal, which we included in the Supporting Information. The combined system presents a number of challenging aspects, for example, the need for controlling the spatial orientation of the crystallographic axis of the nanocrystals relative to the nanoantennas, but also offers an intriguing and extensive parameter space for complex and highly nonlinear hybrid systems as nanoscale coherent light sources, for example, to excite nanoantenna arrays coherently.[54]

■ ASSOCIATED CONTENT

Ⓢ Supporting Information

Figure S1, second harmonic generation on plasmonic bow-tie antennas, which were incorporated with lithium niobate ($LiNbO_3$) nanocrystals. This material is available free of charge via the Internet at http://pubs.acs.org.

■ AUTHOR INFORMATION

Corresponding Author

*(M.H.) E-mail: m.hentschel@physik.uni-stuttgart.de.

Notes

The authors declare no competing financial interest.

■ ACKNOWLEDGMENTS

We gratefully acknowledge financial support from the Baden–Württemberg Stiftung (Kompetenznetz Funktionelle Nanostrukturen), from the DFG (SPP1391, ultrafast nano-optics), from the BMBF (13N10146), and the ERC (Complexplas).

X.Y. and C.B.M.'s contribution to the synthesis and characterization of the ITO nanocrystals was supported by the U.S. Office of Naval Research Multidisciplinary University Initiatives (MURI) program Grant. No. ONR-N00014-10-1-0942. The authors thank Sven Hein for graphical illustrations.

REFERENCES

(1) Mie, G. *Ann. Phys.* **1908**, *330*, 377.
(2) Boyd, R. W. *Nonlinear Optics*, 3rd ed.; Elsevier: New York, 2008.
(3) Campagnola, P. J.; Loew, L. M. *Nat. Biotechnol.* **2003**, *21*, 1356.
(4) Nakayama, Y.; Pauzauskie, P. J.; Radenovic, A.; Onorato, R. M.; Saykally, R. J.; Liphardt, J.; Yang, P. *Nature* **2007**, *447*, 1098.
(5) Hsieh, C.-L.; Grange, R.; Pu, Y.; Psaltis, D. *Opt. Express* **2009**, *17*, 2880.
(6) Alivisatos, A. P. *Nat. Biotechnol.* **2004**, *22*, 47.
(7) Alivisatos, A. P. *Science* **2007**, *271*, 933.
(8) Knabe, B.; Buse, K.; Assenmacher, W.; Mader, W. *Phys. Rev. B* **2012**, *86*, 195428.
(9) Maier, S. A. *Plasmonics: Fundamentals and Applications*; Springer: New York, 2007.
(10) Novotny, L.; van Hulst, N. *Nat. Photonics* **2011**, *5*, 83.
(11) Halas, N. J.; Lal, S.; Chang, W.-S.; Link, S.; Nordlander, P. *Chem. Rev.* **2011**, *111*, 3913.
(12) Giannini, V.; Fernández-Domínguez, A. I.; Heck, S. C.; Maier, S. A. *Chem. Rev.* **2011**, *111*, 3888.
(13) Klein, M. W.; Enkrich, C.; Wegener, M.; Linden, S. *Science* **2006**, *313*, 502.
(14) Zhang, Y.; Grady, N. K.; Ayala-Orozco, C.; Halas, N. J. *Nano Lett.* **2011**, *11*, 5519.
(15) Canfield, B. K.; Husu, H.; Laukkanen, J.; Bai, B.; Kuittinen, M.; Turunen, J.; Kauranen, M. *Nano Lett.* **2007**, *7*, 1251.
(16) Lippitz, M.; van Dijk, M. A.; Orrit, M. *Nano Lett.* **2005**, *5*, 799.
(17) Hanke, T.; Krauss, G.; Träutlein, D.; Wild, B.; Bratschitsch, R.; Leitenstorfer, A. *Phys. Rev. Lett.* **2009**, *103*, 257404.
(18) Danckwerts, M.; Novotny, L. *Phys. Rev. Lett.* **2007**, *98*, 026104.
(19) Biagioni, P.; Brida, D.; Huang, J.-S.; Kern, J.; Duò, L.; Hecht, B.; Finazzi, M.; Cerullo, G. *Nano Lett.* **2012**, *12*, 2941.
(20) Kauranen, M.; Zayats, A. V. *Nat. Photonics* **2012**, *6*, 737.
(21) Khurgin, J. B.; Sun, G. *Opt. Express* **2013**, *21*, 1062.
(22) Raschke, M. B.; Berweger, S.; Atkin, J. M. *Plasmonics: Theory and Applications*; Springer: New York, 2014; Chapter Ultrafast and Nonlinear Plasmon Dynamics.
(23) Kim, S.; Jin, J.; Park, Y.-J.; Kim, Y.; Kim, S.-W. *Nature* **2008**, *453*, 757.
(24) Sivis, M.; Duwe, M.; Abel, B.; Ropers, C. *Nature* **2012**, *485*, E1.
(25) Pfullmann, N.; Waltermann, C.; Noack, M.; Rausch, S.; Nagy, T.; Reinhardt, C.; Kovačev, M.; Knittel, V.; Bratschitsch, R.; Akemeier, D.; Hütten, A.; Leitenstorfer, L.; Morgner, U. *New J. Phys.* **2013**, *15*, 093027.
(26) Niesler, F. B. P.; Feth, N.; Linden, S.; Niegemann, J.; Gieseler, J.; Busch, K.; Wegener, M. *Opt. Lett.* **2009**, *34*, 1997.
(27) Chen, P.; Argyropoulos, C.; Alu, A. *Nanophotonics* **2012**, *1*, 221.
(28) Chen, P.-Y.; Alù, A. *Phys. Rev. B* **2010**, *82*, 235405.
(29) Abb, M.; Albella, P.; Aizpurua, J.; Muskens, O. L. *Nano Lett.* **2011**, *11*, 2457.
(30) Utikal, T.; Zentgraf, T.; Paul, T.; Rockstuhl, C.; Lederer, F.; Lippitz, M.; Giessen, H. *Phys. Rev. Lett.* **2011**, *106*, 133901.
(31) Ueda, N.; Kawazoe, H.; Watanabe, Y.; Takata, M.; Yamane, M.; Kubodera, K. *Appl. Phys. Lett.* **1991**, *59*, 502.
(32) Johnson, P. B.; Christy, R. W. *Phys. Rev. B* **1972**, *6*, 4370.
(33) Mühlschlegel, P.; Eisler, H.-J.; Martin, O. J. F.; Hecht, B.; Pohl, D. W. *Science* **2005**, *308*, 1607.
(34) Hanke, T.; Cesar, J.; Knittel, V.; Trügler, A.; Hohenester, U.; Leitenstorfer, A.; Bratschitsch, R. *Nano Lett.* **2012**, *12*, 992.
(35) Liu, N.; Guo, H.; Fu, L.; Kaiser, S.; Schweizer, H.; Giessen, H. *Nat. Mater.* **2008**, *7*, 31.
(36) Black, C. T.; Murray, C. B.; Sandstrom, R. L. *Embedded Nanoparticle Films and Method for Their Formation in Selective Areas on a Surface*. US Patent US8465829 B2, 2013.
(37) Saboktakin, M.; Ye, X.; Chettiar, U. K.; Engheta, N.; Murray, C. B.; Kagan, C. R. *ACS Nano* **2013**, *7*, 7186.
(38) Choi, S.; Nam, K. M.; Park, B. K.; Seo, W. S.; Park, J. T. *Chem. Mater.* **2008**, *20*, 2609.
(39) Hentschel, M.; Utikal, T.; Giessen, H.; Lippitz, M. *Nano Lett.* **2012**, *12*, 3778.
(40) Niesler, F. B. P.; Feth, N.; Linden, S.; Wegener, M. *Opt. Lett.* **2011**, *36*, 1533.
(41) Zuloaga, J.; Nordlander, P. *Nano Lett.* **2011**, *11*, 1280.
(42) Alonso-González, P.; Albella, P.; Neubrech, F.; Huck, C.; Chen, J.; Golmar, F.; Casanova, F.; Hueso, L. E.; Pucci, A.; Aizpurua, J.; Hillenbrand, R. *Phys. Rev. Lett.* **2013**, *110*, 203902.
(43) Metzger, B.; Hentschel, M.; Lippitz, M.; Giessen, H. *Opt. Lett.* **2012**, *37*, 4741.
(44) Refractive index database. http://refractiveindex.info.
(45) Linden, S.; Niesler, F. B. P.; Förstner, J.; Grynko, Y.; Meier, T.; Wegener, M. *Phys. Rev. Lett.* **2012**, *109*, 1.
(46) Metzger, B.; Schumacher, T.; Hentschel, M.; Lippitz, M.; Giessen, H. Submitted.
(47) Sönnichsen, C.; Franzl, T.; Wilk, T.; von Plessen, G.; Feldmann, J. *Phys. Rev. Lett.* **2002**, *88*, 077402.
(48) Aouani, H.; Rahmani, M.; Navarro-Cía, M.; Maier, S. A. *Nat. Nanotechnol.* **2014**, *9*, 290.
(49) Zhang, Y.; Wen, F.; Zhen, Y.-R.; Nordlander, P.; Halas, N. J. *Proc. Natl. Acad. Sci. U.S.A.* **2013**, *110*, 9215.
(50) Aouani, H.; Navarro-Cia, M.; Rahmani, M.; Sidiropoulos, T. P. H.; Hong, M.; Oulton, R. F.; Maier, S. A. *Nano Lett.* **2012**, *12*, 4997.
(51) Tinguely, J.-C.; Sow, I.; Leiner, C.; Grand, J.; Hohenau, A.; Felidj, N.; Aubard, J.; Krenn, J. R. *BioNanoScience* **2011**, *1*, 128.
(52) Birss, R. R. *Symmetry and Magnetism*; North-Holland Publishing Co.: Amsterdam, The Netherlands, 1966.
(53) Gentile, M.; Hentschel, M.; Taubert, R.; Guo, H.; Giessen, H.; Fiebig, M. *Appl. Phys. B: Laser Opt.* **2011**, *105*, 149.
(54) Dregely, D.; Taubert, R.; Dorfmüller, J.; Vogelgesang, R.; Kern, K.; Giessen, H. *Nat. Commun.* **2011**, *2*, 267.